SOFC Modeling - From Micro-Kinetics to Stacks

Olaf Deutschmann, Vinod Janardhanan, Steffen Tischer, Vincent Heuveline
Universität Karlsruhe (TH)
Institute for Chemical Technology & Polymer Chemistry
Engesserstr. 20
76131 Karlsruhe, Germany
Tel: +49-721-608 3138
olaf.deutschmann@kit.edu

Abstract

This paper presents a hierarchical modeling approach for Solid-Oxide Fuel Cells from elementary kinetics to stacks. On a fundamental level, we have developed an analytical model for the evaluation of volume specific three-phase boundary length (vL_{tpb}) in composite electrodes and electrochemical kinetics expressions to account for coverage dependent activation energies of various surface adsorbed species. The kinetics are applied for modeling SOFCs operating on various reformate compositions. The results of both fundamental modeling approaches are compared with experimental data [1, 2]. On an application level, a novel approach for modeling a SOFC stack is presented. The approach is based on decoupling heat transfer from the other processes [3] and a newly developed cluster agglomeration algorithm, which drastically reduces the computational costs associated with stack simulation. Based on the assumption that all unit cells with similar temperature profiles behave alike, the cells are divided into clusters according to differences in their local temperature profiles. All unit cells of one cluster are then represented by one cell, for which a simulation is conducted, which applies detailed models for electro-chemical conversion at the three-phase boundary, an elementary-step reaction mechanism for the thermo-catalytic conversion of the fuel on the catalyst in the anode [4], dusty-gas model to account for multi-component diffusion and convection in the electrodes, and a plug-flow model for the flow in the fuel and air channels.

1. Introduction

Currently SOFCs running on multi-component fuel mixtures are receiving special attention [5-9]. Extensive research has been subjected to run diesel or gasoline reformate on SOFCs. However, these reformate will essentially be a fuel mixture of hydrocarbons and syngas [10, 11]. Depending on the conditions in the fuel reformer, CO_2/H_2O can also be present in the reformate fuel. Under these circumstances, the accuracy of an SOFC model depends largely on coupled interactions of heterogeneous chemistry and electrochemistry. Although SOFC numerical models can throw great insight into details of physico-chemical processes occurring in the cell, the performance of the cell largely depends on the materials, manufacturing conditions, and the resulting microstructure of the cell components. In-order to cover the aspects ranging from microstructures to stacks, this paper is organized into three major sections namely (1) electrode micro-structure, (2) heterogeneous charge transfer model, and (3) stack model.

2. Electrode microstructure

The performance of an SOFC largely depends on the microstructure of the resulting electrodes and the processing conditions. The electrochemical charge transfer reactions proceeds at the three-phase interfaces (TPB). In a composite electrode, normally the active TPB region spreads to a few microns (10-15 μm) in the vicinity of electrode-electrolyte interface. Wilson et al. [1] reported the three-dimensional reconstruction of a SOFC anode using ion-beam scanning electron microscopy to determine the micro-structural properties. They estimated the volume-specific TPB length for their sample to be 4.28×10^{12} m/m^3. Brown et al. [12] reported that Ni forms larger particles with the particle sizes ranging from 0.5 to 3.0 μm, while YSZ phase particle size distribution were 0.5-1.0 μm. Hence, we need to consider the volume specific TPB length for cases with two mono-sized particle distributions. Schneider et al. [13] reported the discrete modeling of composite electrode and developed an analytical model for calculating the TPB length.

The model presented here is developed by considering a geometric volume of a composite electrode characterized by its porosity and particle radii r_1 and r_2. We start the model development by considering the intersection of two spherical particles as shown in Fig 1.

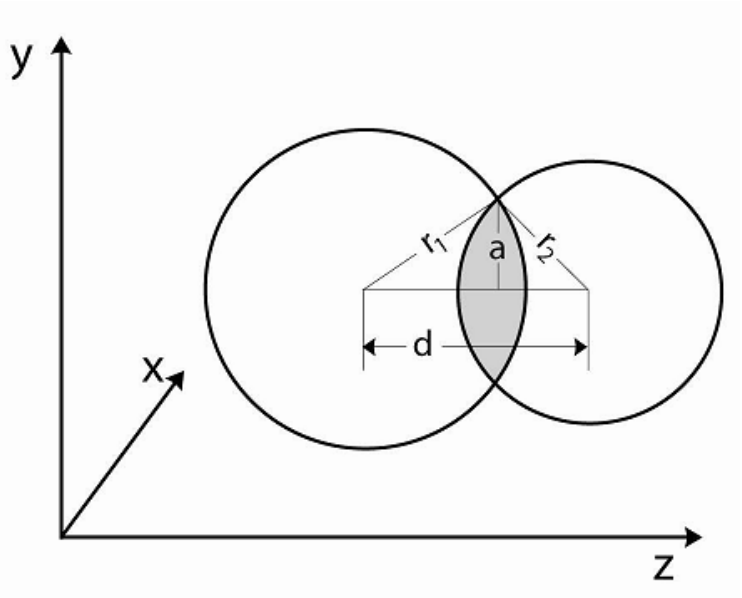

Figure 1: Intersection of two spherical particles.

The volume of the three dimensional lens common to both the spheres as a result of intersection is given by

$$V_l = \frac{\pi(r_1 + r_2 - d)^2(d^2 + 2dr_2 - 3r_2^2 + 2dr_1 + 6r_2r_1 - 3r_1^2)}{12d}. \quad (1)$$

Further the intersection of the spheres is a curve lying in the plane parallel to the x-plane whose radius *a* is given by

$$a = \frac{1}{2d}\sqrt{4d^2r_1^2 - (d^2 - r_2^2 + r_1^2)^2}\ . \quad (2)$$

The total volume loss V_{tl} as a result of intersection is given by

$$V_{tl} = N_p(1-\psi)V_l\,. \tag{3}$$

Here, ψ is the fractional overlap and N_p is the number of particles. If we assume the electronic and ionic particles are of different average sizes with radii r_1 and r_2, then the ratio between the number of particles *M* can be defined as

$$M = \frac{N_{p2}}{N_{p1}} = \frac{\phi_2 r_1^3}{\phi_1 r_2^3} \tag{4}$$

with ϕ_1 and ϕ_2 as volume fraction of particles with radii r_1 and r_2, respectively. Let V_t be the total volume of the electrode under consideration then, the total solid volume V_t can be expressed as

$$(1-\phi)V_t = N_{p1}\frac{4}{3}\pi r_1^3 + N_{p2}\frac{4}{3}\pi r_2^3 - (N_{p1}+N_{p2})(1-\psi)V_l\,, \tag{5}$$

ϕ is the gas-phase porosity. Combining the above equations, the total number of particles can be written as

$$N_p = \frac{(1-\phi)V_t(1+M)}{\frac{4}{3}\pi(r_1^3 + Mr_2^3) - (1-\psi)(1+M)V_l}\,. \tag{6}$$

The length of boundary due to the intersection of two spheres is given by the circumference of a circle. This becomes a three-phase boundary length (TPB) only if the intersecting particles are of different phases and the intersection is associated with a pore space. Therefore, the average TPB length of the composite electrode is given by

$$L_{tpb} = N_p \min\left\|Z_{i-e}, Z_{e-i}\right\| \phi 2\pi a\,, \tag{7}$$

Z_{i-e} is the coordination number between the ionic and electronic conductors and Z_{e-i} is the coordination number between the electronic and ionic conductors. The average number of contacts between the ionic and electronic conducting particle is given by

$$Z_{i-e} = \phi_e \frac{Z_i Z_e}{Z}\,, \tag{8}$$

and the average number of contacts between the electronic and ionic conducting particle is given by

$$Z_{e-i} = \phi_i \frac{Z_i Z_e}{Z}\,. \tag{9}$$

Here, Z is the average co-ordination number. Expressions for Z_i and Z_e are given in [14]. Combination of Eqs. (6) and (7) leads to the volume specific three-phase boundary length vL_{tpb}:

$$vL_{tpb} = \frac{\phi(1-\phi)(1+M)\min\left\|Z_{i-e}, Z_{e-i}\right\|2\pi a}{\frac{4}{3}\pi(r_1^3 + Mr_2^3) - (1-\psi)(1+M)V_l}. \quad (10)$$

In the case of mono-sized particles vL_{tpb} is given by

$$vL_{tpb} = \frac{\phi(1-\phi)\min\left\|Z_{i-e}, Z_{e-i}\right\|2\pi a}{\frac{4}{3}\pi r^3 - (1-\psi)V_l}. \quad (11)$$

The model presented here is developed by considering a geometric volume of a composite electrode characterized by its porosity ϕ and particle radii r_1 and r_2. It is assumed that the ionic and electronic solid phases are made up of spherical particles.

3. Heterogeneous charge transfer model

Most SOFC modeling efforts employ Nernst equation to calculate the open circuit potential and Butler-Volmer equation to express the rate of charge transfer reaction. However, Butler-Volmer equation does not throw any insight into the actual process occurring on the surface which leads to electron transfer near the TPB. Here we present an electrochemistry model based on heterogeneous chemistry occurring at the TPB. A detailed version of the following discussions will be published elsewhere [15].

The forward and reverse rate constants for charge transfer reaction are written as

$$k_{fi} = k_{fi}^0 \exp(z\frac{\alpha_a F}{RT}\Delta\phi) \text{ and} \quad (12)$$

$$k_{ri} = k_{ri}^0 \exp(-z\frac{\alpha_c F}{RT}\Delta\phi), \quad (13)$$

respectively. Here $\Delta\phi$ is the potential between Ni and YSZ phases. k_{fi}^0 and k_{ri}^0 are the forward and backward thermal rate coefficients, which can be expressed in terms of modified Arrhenius expression as

$$k_{fi}^0 = A_{fi}T^{\beta i}\exp(-\frac{E_{fi}}{RT})\prod_{k=1}^{K_s}\exp(-\frac{\varepsilon_k\theta_k}{RT}) \quad (14)$$

$$k_{ri}^0 = A_{ri}T^{\beta i}\exp(-\frac{E_{ri}}{RT})\prod_{k=1}^{K_s}\exp(-\frac{\varepsilon_k\theta_k}{RT}) \quad (15)$$

Here θ_k is the surface coverage of the k-th species and ε_k is a parameter modelling coverage dependency of activation energy. All other parameters have the usual meaning. The faradic current for the i-th charge transfer reaction can then be given as

$$i_i = zFL_{tpb}\left[k_{fi}\prod_{k=1}^{K_s}\theta_k^{\upsilon'} - k_{ri}\prod_{k=1}^{K_s}\theta_k^{\upsilon''}\right] \tag{16}$$

Here L_{tpb} is the area specific TPB length, K_s is the total number of surface species and υ' and υ'' are the stoichiometric coefficients of the reactants and products, respectively. Based on the above equation the total Faradic current is written as

$$i = \sum_{i=1}^{N_{ct}} i_i\,, \tag{17}$$

N_{ct} is the total number of charge transfer reactions. Based on the potential difference between the electronic and ionic phases, the operating cell potential can be expressed as

$$E_{cell} = \Delta\phi_c - \Delta\phi_a - \eta_{ohm} \tag{18}$$

$\Delta\phi_c$ and $\Delta\phi_a$ are respectively the potential difference on the cathode and anode side.

The following electrochemical reactions are considered for evaluating the model with experimental measurements:

$$2\mathrm{H[Ni]} + \mathrm{O[YSZ]}^{2-} \leftrightarrow \mathrm{H_2O[YSZ]} + 2\mathrm{[Ni]} + 2\mathrm{e}^- \tag{19}$$

$$\mathrm{CO[Ni]} + \mathrm{O[YSZ]}^{2-} \leftrightarrow \mathrm{CO_2[YSZ]} + \mathrm{[Ni]} + 2\mathrm{e}^- \tag{20}$$

$$\mathrm{O}^{\mathrm{x}}\mathrm{[el]} \leftrightarrow \frac{1}{2}\mathrm{O_2} + \mathrm{V_o^{\bullet\bullet}} + 2\mathrm{e}^-\,. \tag{21}$$

4. Stack model

The timescales of various processes such as kinetics, diffusion, and heat transfer occurring in an SOFC stack are different from each other, and the heat transfer process has a larger time constant compared to the rest of the processes. In the method adopted here, the solid-phase temperature is decoupled from the fluid phase to develop the transient stack model, which solves the transient two or three-dimensional heat conduction problem. While solving the heat conduction equation, the stack is assumed as a porous media, consisting of straight channels. The heat balance can then be written as

$$\rho C_p \frac{\partial T}{\partial t} = \frac{\partial}{\partial x_i}\left(\lambda_{ij}\frac{\partial T}{\partial x_j}\right) + q \tag{22}$$

Here, t = time, T = temperature, ρ = density, C_p = heat capacity, λ_{ij} = tensor of heat conductivity; q is the heat source term arising from the interaction with the individual cells. The heat source term is derived from the simulation of individual cells. If the cell density is σ (cells per unit area of the cross-section), the source term can be expressed as

$$q = -\sigma\frac{\partial H_{\mathrm{cell}}}{\partial x} + Q_{\mathrm{ohm}} \tag{23}$$

H_{cell} is the enthalpy flux in the cell and Q_{ohm} is the heat release due to ohmic heating. The cell model is used for simulations as reported in [4]. A cluster agglomeration algorithm is

applied to choose the representative cells from the individual cells following the strategy developed before for transient simulations of catalytic monoliths [18, 19]. More details of the stack model will be published elsewhere [20].

5. Results and Discussion

5.1 Electrode microstructure

The following results are presented for mono sized particles for both ionic as well as for electronic phases. Quite obviously Eq. (11) predicts maximum volume specific TPB length (vL_{tpb}) at 50% porosity while other parameters are fixed. Figure 2 displays the influence of grain size on vL_{tpb} as a function of gas-phase porosity ϕ. As predicted by Eq.17, maximum vL_{tpb} is observed at 50% porosity for all the grain sizes considered and the vL_{tpb} increases with decreasing grain size. For the results presented in Fig. 2, the average distance between the particles is assumed to be 1 μm and a coordination number ($Z_{i-e} = Z_{e-i}$) of 7.2 is used. From the order of magnitude the results are in good agreement with the experimental evaluation of vL_{tpb} by Wolson et al. [1]. More discussions on the application of the vL_{tpb} model are published elsewhere [14].

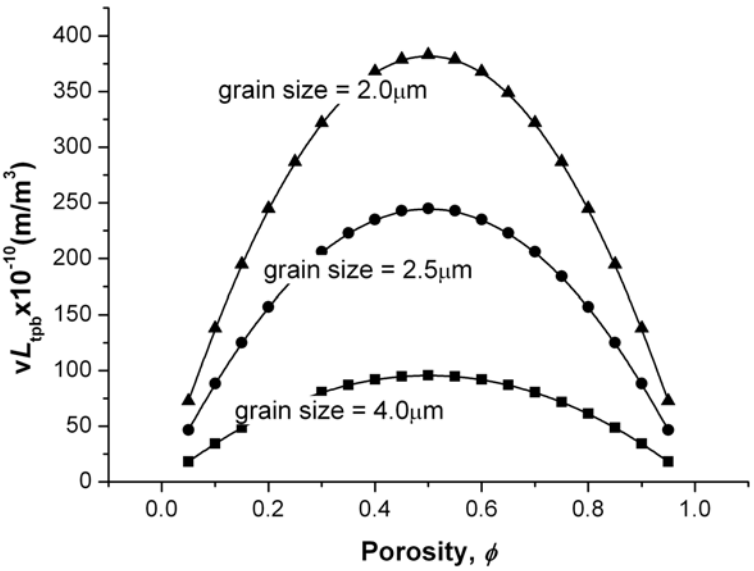

Figure 2: TPB length as a function of porosity for various grain sizes.

5. 2 Heterogeneous charge transfer model

A heterogeneous reaction mechanism consisting of 42 reactions among 6 gas-phase species and 12 surface adsorbed species used throughout this work and is reported in [16]. The pure H_2 operated cell is first modeled by fitting the pre-exponential factor and coverage dependent activation energy. The fit parameters for the electrochemistry model are given in Table.1

Table 1: Parameters for electrochemistry model

H_2 Oxidation	
Activation energy (kJ/mol)	89.4
Pre exponential factor (mol/cm-s)	8.5×10^{-2}
Coverage dependent activation energy for H (kJ/mol)	-10.0
Coverage dependent activation energy for H2O (kJ/mol)	-30.0
CO Oxidation	
Activation Energy(kJ/mol)	60.0
Pre exponential (mol/ cm-s)	4.00×10^{-4}
Coverage dependent activation energy for CO(kJ/mol)	-10.0
Order dependency on CO_2 coverage	4
O_2 Reduction	
Activation energy (kJ/mol)	120.0
Pre exponential (mol/cm-s)	1.5×10^{-2}

Comparison between the simulated curve and the experimentally observed one for pure H_2 operated cell is shown in Fig. 3. The model predicts higher peak power density compared to the experimental observation. Experimentally peak power density of 1.61 W/cm^2 is observed at 3.22 A/ cm^2, while, the simulation yield 1.81 W/ cm^2 at 3.46 A/ cm^2. Although it is quite possible to reproduce the same experimental observation quantitatively, we did not resort to that since the fitted parameters adversely affected the model prediction on the performance on reformate fuel compositions.

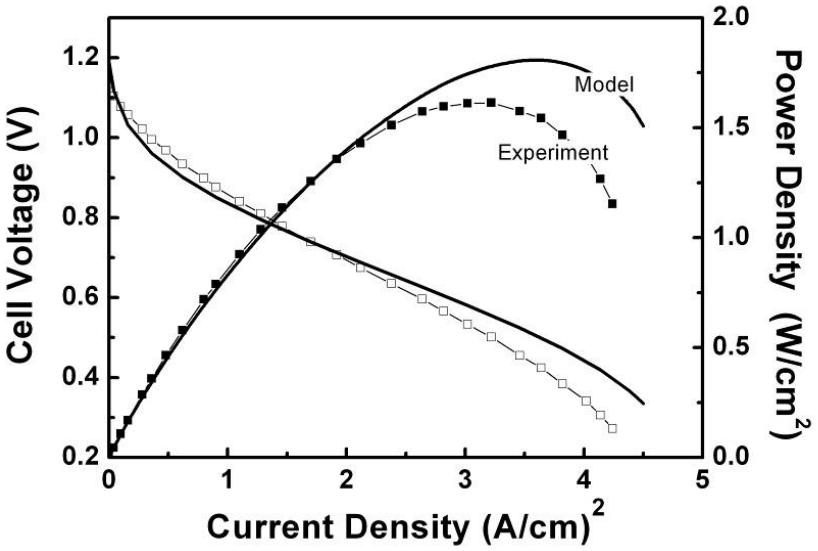

Figure 3: Comparison of model prediction with cell performance on pure H_2.

Figures 4(a) and 4(b), display the experimentally observed and simulated performance curves, respectively, for a cell operated with the reformate fuel resulting from the partial oxidation of methane using air. The details of fuel composition are given in [2]. Experimentally CH_4:air ratio of 60:20 gave the best performance with a limiting current of ~4.0 A/cm^2. The simulations lead to a limiting current of ~3.25 A/ cm^2 for the same fuel composition. For CH_4:air ratio of 40:100 the simulations predicted a limiting current of ~2.08 A/ cm^2, while the experimentally observed value is ~2.5 A/cm^2. In general the limiting currents are slightly under predicted by the simulations, and the peak power densities are predicted within a relative error of ~14%.

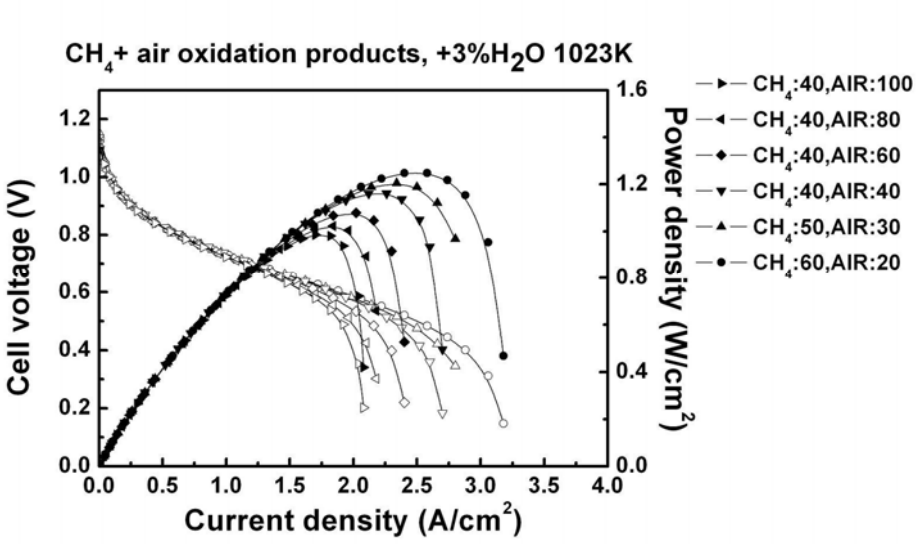

Figure 4(a): Experimentally measured cell performance with H_2 and reformer fuel from the POM with air diluted with 3% H_2O (Reproduced from [2]).

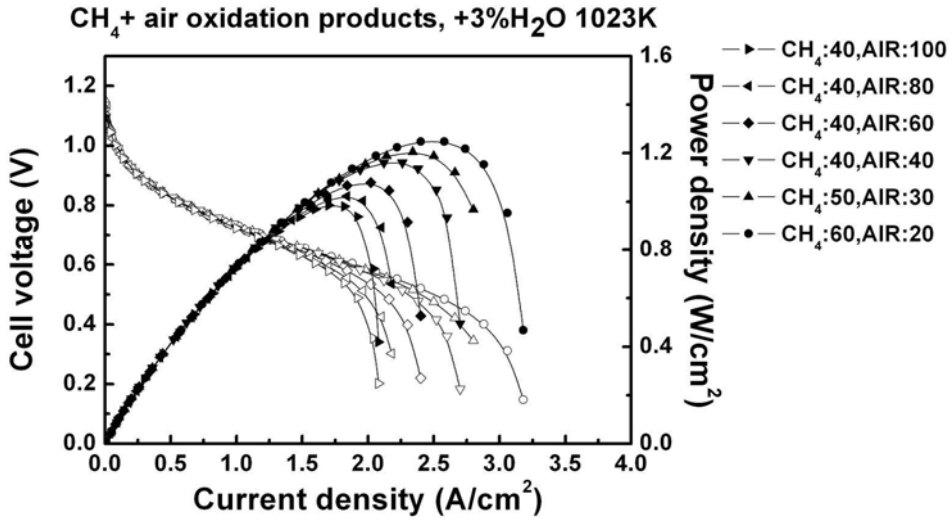

Figure 4(b): Simulated cell performance with reformer fuel from the POM with air diluted with 3% H_2O.

5.3 Stack model

For demonstration purposes, we consider a stack having active area of 10 cm ×10 cm, and consisting of 30 cells in co-flow configuration. The anode, cathode, and electrolyte components are assumed to be 750 μm, 30 μm, and 15 μm thick, respectively. The fuel and air channels are assumed to be of 1 mm^2 cross sectional area. The inlet fuel composition considered is 31.81% H_2, 13.19% CO, 13.19% CH_4, 2.23% CO_2, 3% H_2O, and 36.58% N_2. Inlet fuel and air are assumed to be at 800 °C and 750 °C, respectively. The exchange current density formulations are taken from [17]. However, the exchange current density parameters are adjusted to produce ~0.72 V at 300 mA/cm^2. Adiabatic boundary conditions are implemented for the calculation.

The temperature distribution in the stack at different planes along and across the flow direction after the first steady state is displayed in Fig. 5. As expected the temperature in

the stack increases along the flow direction due to the exothermic cell reactions. However, uniform profiles are observed across the direction of flow. It should be noticed that the model has the limitation that it does not account for the individual mechanical components in the stack. It is a lumped parameter model as far as the individual mechanical components are concerned and therefore, uniform thermal properties are assumed everywhere in the stack.

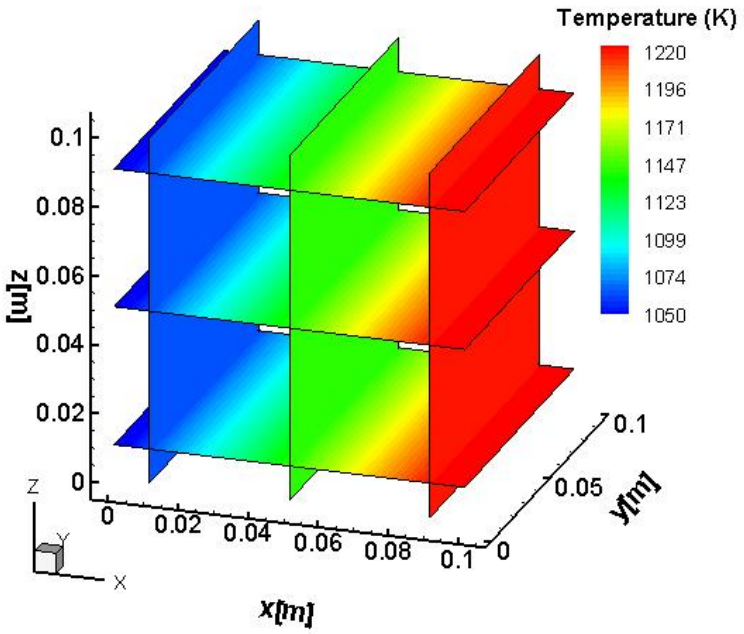

Figure 5: Temperature distribution in the 3D stack (solid phase) at different surface planes along and across the flow direction (average current density = 300 mA/cm^2)

6. Conclusions

We have developed an analytical expression for the evaluation of volume specific three-phase boundary length in SOFC electrodes. The model predictions are in good agreement with experimental observations. Furthermore, the model is also applicable to cases where the constituent particles are of different size distribution.

The electrochemical model presented takes into account multiple charge transfer reactions and coverage dependant activation energy for various surface adsorbed species taking part in the charge transfer reaction. The model predictions are in reasonable agreement with experimental observations.

The stack model presented here is based on a cluster agglomeration algorithm in choosing the representative cells for detailed calculation. The approach considerably reduces the calculation time.

References

(1) J. R.Wilson, W. Kobsiriphat, R. Mendoza, H.Y. Chen, J. M.Hiller, D.J. Miller, K. Thornton, P.W. Voorhees, S. B. Adler, S. A. Barnett. Nature Materials, 5 (2006) 541-544

(2) B. Tu, Y. Dong, M. Cheng, Z. Tian, Q. Xin. Natural Gas Conversion VIII, Studies in Surface Science and Catalysis 167, M. Schmal, F.B. Noronha, E. F. Sousa-Aguiar (eds.), p. 43-48, Elsevier, 2007

(3) E. Achenbach. J. Power Sources 57 (1995) 105-109

(4) H. Zhu, R.J. Kee, V.M. Janardhanan, O. Deutschmann, D.G. Goodwin. J. Electrochem. Soc. 152 (2005) A2427-A2440

(5) E. P. Murray, T. Tsai, S. A. Barnett. Nature 400 (1999) 649

(6) Z. Cheng, S. Zha, L. Aguilar, D. Wand. Electrochem. Solid State Lett. 9 (2006) A31

(7) Y. Lin, Z. Zhan, J. Liu, S.A. Barnett. Solid State Ionics 176 (2005) 1827

(8) J. Liu, S.A. Barnett. Solid State Ionics 158 (2003) 11

(9) B.C.H. Steele. Nature 400 (1999) 619

(10) I. Kang, J. Bae, G. Bae. J. Power Sources 163, (2006) 538

(11) T. Aicher, L. Griesser. J. Power Sources 165 (2007) 210

(12) M. Brown, S. Primdahl, M. Mogensen. J. Electrochem. Soc.,147 (2000) 475

(13) L. Schneider, C. Martin, Y. Bultel, D. Bouvard, E. Siebert. Electrochimica Acta 52 (2006) 314

(14) V. M. Janardhanan, V. Heuveline, O. Deutschmann, J. Power Sources 178 (2008) 368-372

(15) V. M. Janardhanan, S. Tischer, V. Heuveline, B. Tu, M. Cheng, O. Deutschmann, J. Electrochem. Soc. (submitted)

(16) V. M. Janardhanan, O. Deutschmann. Zeitschrift f. Phys. Chem. 221 (2007) 443

(17) V. M. Janardhanan, O. Deutschmann J. Power Sources 162 (2006) 1192–1202

(18) S. Tischer, O. Deutschmann. Catalysis Today 105 (2005) 407-413

(19) O.Deutschmann, S. Tischer, S. Kleditzsch, V.M. Janardhanan, C. Correa, D. Chatterjee, N. Mladenov, H. D. Mihn, DETCHEM Software package, 2.1 ed., www.detchem.com, Karlsruhe 2007.

(20) V. M. Janardhanan, S. Tischer, V. Heuveline, O. Deutschmann, J. Power Sources (to be submitted)